Localization and Tracking in mmWave Radio Networks using Beam-Based DoD Measurements

Elizaveta Rastorgueva-Foi*, Mário Costa†, Mike Koivisto*, Kari Leppänen†, and Mikko Valkama*
* Laboratory of Electronics and Communications Engineering, Tampere University of Technology, Finland
† Huawei Technologies Oy (Finland) Co., Ltd, Finland
Email: elizaveta.rastorgueva-foi@tut.fi

***Abstract*—3D-beamforming capabilities of multiantenna equipments in fifth generation (5G) networks, operating in the millimeter wave (mmW) band, allow for accurate positioning and tracking of users. In this paper, we propose a method for 3D positioning and tracking of moving user equipments (UEs) in 5G mmW networks based on downlink (DL) reference signals (RSs) and maximum ratio combining of subcarriers. In particular, we consider a system where base stations (BSs) transmit beamformed DL RSs in a periodic manner and UEs exploit such RSs for estimating the BS-UE beam-pair gains by coherently combining all of the available subcarriers. This is achieved by a novel maximum likelihood (ML) estimator for the beam-pair gain. These beam-pair gain estimates are then reported back to the BSs, where they are used to estimate the direction of departure (DoD) of the DL RSs by a novel extended Kalman filter (EKF). The obtained DoD estimates from all available BSs are fused into a UE position estimate in a central unit of the considered network by a second stage EKF. Hence, the computational burden is distributed among different network entities. The proposed positioning algorithm may be implemented with minor modifications to the signalling scheme currently specified for the first phase (Rel. 15) of of 3GPP 5G New Radio (NR) systems. The performance of this positioning scheme is evaluated in a realistic ray-tracing based outdoor scenario mimicking an automated truck platooning in a cargo port setting.**

***Index Terms*—positioning, localization, tracking, 5G networks, IoT, automatic platooning, beamforming, direction-of-departure, location-awareness, extended Kalman filter, line-of-sight**

I. Introduction

Fifth generation (5G) wireless networks are expected to adopt millimeter wave (mmW) frequency bands, in which more bandwidth is available, in order to cope with the ongoing growth of mobile traffic. Exploiting mmW bands not only increases capacity, but also allows for new opportunities for highly accurate user equipment (UE) positioning. In fact, a recent 3GPP study item proposes a radio access technology (RAT)-dependent solution for 5G positioning [1], [2]. In particular, transmit and receive beamforming is expected to be employed in 5G base stations (BSs) and UEs operating at mmW frequencies in order to counteract the considerable path loss at these bands [3], [4]. Directional transmissions at the BSs can also be used for determining the directions of departure (DoDs) of downlink (DL) signals, which in turn may be used for 3D positioning of UEs.

In this paper, building on the premises of mmW 5G small cell networks with directional transmission and reception, we propose a scheme where the 3D positions of UEs are estimated and tracked by means of sequential extended Kalman filters (EKFs) and maximum ratio combining of available subcarriers. This is an extension of our work in [5] in which a positioning scheme based on a Gaussian approximation of reference signal received power (RSRP) measurements was proposed. Herein, such an approximation of the beam-pair gain is not required, but this is achieved at the cost of increased complexity at the UE and a calibrated transmitter (Tx)-receiver (Rx) frequency-response. The latter can be avoided by employing a narrowband frequency-flat system. In particular, we consider a system in which each BS transmits beamformed DL reference signals (RSs) that are measured by UEs, similarly employing receive beamforming. In the proposed positioning algorithm, UEs coherently combine the DL-RSs modulating multiple subcarriers, and estimate the gain of each beam-pair using a novel maximum likelihood estimator (MLE). The estimated beam-pair gains for the strongest (or most reliable) UE beams are then communicated back to the BSs. Then, a novel two-stage EKF is employed to sequentially estimate the 3D position of UEs. More precisely, the first-stage EKF estimates the DoDs of DL RSs based on feedback beam-pair gain estimates. Finally, the UE-specific DoD estimates from all the available BSs are fused at a central entity by a second-stage EKF into a 3D position estimate.

The proposed 3D positioning scheme is evaluated in a framework resembling that of truck platooning. A (truck) platoon is a string of vehicles driving along the same trajectory with short gaps between each other, connected via vehicle to vehicle (V2V) or vehicle to everything (V2X) data communication [6], [7]. The leading truck may be either human-driven or driverless. Platooning aims at energy saving due to reduced aerodynamic drag, thus leading to minimization of the fuel consumption and subsequent CO_2 emission, as well as increase in the road capacity without jeopardizing safety. Another advantage of truck platooning is the mitigation of skilled drivers' shortage and future labour costs savings. Each platoon member is equipped with various sensors to be able to keep lane, control its speed, avoid collisions and keep a gap between each other, with the latter being the crucial function for energy saving.

This work was supported by the Doctoral Program of the President of Tampere University of Technology, the Tuula and Yrjö Neuvo Fund, the Nokia Foundation, and the Finnish Funding Agency for Technology and Innovation (Tekes), under the projects "TAKE-5: 5th Evolution Take of Wireless Communication Networks", and "WIVE: Wireless for Verticals".

Lateral control is performed with road marker sensors (typically optical), whereas longitudinal control i.e., maintaining the speed and the gap between trucks, is based on fusion from multiple sensors (typically a radar, a lidar and/or a CMOS camera) as well as V2V communication communication for the transfer of necessary data between platoon members [6], [8]. Also, V2X communication is often used as an additional sensor [7]. The truck separation in the platoon is a key parameter: small gap yields large fuel reduction compared to conventional truck operations. In most platooning tests the clearance gap was kept in the range of $5-10$ m [6], which corresponds to the delay of <1 s between the trucks. However, it should be noted that precise energy saving gains depend also on the speed and the place of the truck within the platoon [6].

One application of above truck platooning is automated hauling and docking of freight containers at maritime cargo terminals. In fact, the Singapore Ministry of Transport and the Port of Singapore Authority have already begun to develop a track platooning system [9] to increase the productivity of the port facilities and to address the shortage of highly-skilled drivers. It should be noted that the aerodynamic drug reduction is not a main objective in this low-speed application. However, cargo terminals, alongside other places where goods are stored and moved, are often envisioned as likely locations for the deployment of industrial Internet-of-Things (IoT) based on mmW wireless network that can be employed for the precise user positioning. In case all platoon members are equipped with 5G transceivers, the 5G wireless network could provide a V2X communication channel, and highly accurate network positioning can assist in the longitudinal control of the platoon. We therefore evaluate the proposed positioning scheme in a settings resembling a cargo terminal.

This paper may be understood as an extension of our work in [5] by considering maximum ratio combining of subcarriers. In particular, the positioning scheme in [5] is based on a Gaussian approximation of (feedback) beam-RSRP measurements whereas in this paper such an approximation of the beam-pair gain is not required. This comes at the expense of increased complexity at the UE and a calibrated Tx-Rx frequency-response. The latter can be avoided by employing a narrowband frequency-flat system in terms of the reference symbol allocation for positioning.

The rest of the paper is organized as follows. First, the considered system model is given in Section II. In Section III, the maximum likelihood (ML) estimator of BS-UE beam-pair gain is proposed. Section IV provides the considered two-stage EKF solution, namely, the direction of departure (DoD) tracking EKF running at BSs and UE positioning EKF operating at a central entity. The considered deployment scenario as well as results of the simulations and numerical evaluations are presented in Section V. Finally, Section VI concludes the paper.

II. System Model

Let $\boldsymbol{y}_{i,j} \in \mathbb{C}^{\mathcal{M}_f}$ denote the multicarrier observation in an orthogonal frequency-division multiplexing (OFDM) system at the UE side. The subscripts i,j refer to the ith UE Rx beam and the jth BS Tx beam, and $\mathcal{M}_f$ denotes the number of subcarriers. Assuming a single dominant line-of-sight (LoS) path, the multicarrier observation at the UE is given by

$$\boldsymbol{y}_{i,j} = \boldsymbol{S}\boldsymbol{b}_f(\tau_{i,j}) b^i_{\mathrm{UE}}(\vartheta_a,\varphi_a) b^j_{\mathrm{BS}}(\vartheta_d,\varphi_d)\gamma_{i,j} + \boldsymbol{n}_{i,j}, \quad (1)$$

where $\boldsymbol{S} \in \mathbb{C}^{\mathcal{M}_f \times \mathcal{M}_f}$ is a diagonal matrix denoting the transmitted symbols in frequency domain, and $\boldsymbol{b}_f(\tau_{i,j}) \in \mathbb{C}^{\mathcal{M}_f}$ denotes the combined frequency-response of the channel and Tx-Rx radio frequency (RF)-chains. Moreover, $b^j_{\mathrm{BS}}(\vartheta_d,\varphi_d) \in \mathbb{C}$ and $b^i_{\mathrm{UE}}(\vartheta_a,\varphi_a) \in \mathbb{C}$ denote the complex-valued beampatterns of the jth BS and ith UE beams, respectively. Note that Tx and Rx are assumed to transmit and receive single-polarized (e.g., vertically-polarized) signals, respectively. Throughout this paper, the departure elevation and azimuth angles at the BS are denoted as (ϑ_d,φ_d), whereas the arrival elevation and azimuth angles at the UE are denoted as (ϑ_a,φ_a). The propagation delay between the ith UE Rx beam and the jth BS Tx beam, including clock-offsets, is denoted by $\tau_{i,j}$. Finally, $\gamma_{i,j} \in \mathbb{C}$ denotes the (vertically-polarized) channel's path-weight between the ith UE Rx beam and the jth BS Tx beam [10], [11], while $\boldsymbol{n}_{i,j} \in \mathbb{C}^{\mathcal{M}_f}$ denotes measurement noise. In particular, we assume that $\boldsymbol{n}_{i,j} \sim \mathcal{N}_C(\boldsymbol{0}, \sigma^2_{i,j}\boldsymbol{I})$ as well as $\mathbb{E}\{\boldsymbol{n}_{i,j}\boldsymbol{n}^H_{k,l}\} = \boldsymbol{0}$ when $i \neq k$. In other words, we assume a noise-limited system and a radio channel with negligible diffuse scattering. The assumption of uncorrelated measurement noise holds when the UE beams are formed at different time-instants, employ different RF-chains, or the beams are orthogonal. These assumptions typically hold in mmW systems.

The combined frequency-response of the channel and Tx-Rx RF-chains, denoted by $\boldsymbol{b}_f(\tau_{i,j})$, is modeled as [11, Ch.2]

$$\boldsymbol{b}_f(\tau_{i,j}) = \boldsymbol{G}_f[\mathrm{e}^{-\mathrm{j}2\pi\frac{\mathcal{M}_f-1}{2}f_0\tau_{i,j}}, \ldots, \mathrm{e}^{\mathrm{j}2\pi\frac{\mathcal{M}_f-1}{2}f_0\tau_{i,j}}]^T, \quad (2)$$

where $f_0 \in \mathbb{R}$ and $\boldsymbol{G}_f \in \mathbb{C}^{\mathcal{M}_f \times \mathcal{M}_f}$ denote the subcarrier spacing and the combined frequency-response of the Tx-Rx RF-chains, respectively. We assume that $\boldsymbol{G}_f$ has either been acquired by e.g., over-the-air calibration, or is essentially constant (i.e., frequency-flat RF-chains) over the operating bandwidth of the reference symbols.

We now consider two limitations typically found in practice. Firstly, the UE's Rx beam characteristics are either not available at the network side or the capacity of the feedback channel does not allow for reporting all $\mathcal{M}_{\mathrm{BS}} \times \mathcal{M}_{\mathrm{UE}}$ channels, where $\mathcal{M}_{\mathrm{BS}}$ and $\mathcal{M}_{\mathrm{UE}}$ denote the number of beams at a given BS and UE, respectively. Hence, we focus on estimating the DoD of the DL LoS path. Note that both DoD and direction of arrival (DoA) may be estimated given that all of the $\mathcal{M}_{\mathrm{BS}} \times \mathcal{M}_{\mathrm{UE}}$ channels are available at the BS. Secondly, the relative phases among the BS Tx beams are unknown (e.g., uncalibrated system). Hence, we focus on acquiring the gains of BSs' DL beams for DoD estimation and subsequent UE positioning.

In particular, the UE positioning task proposed in this paper consists in the following three main steps (see also Fig. 1):

- UEs estimate the gains of BSs' DL beams using known RSs by coherently combining the measured subcarriers.

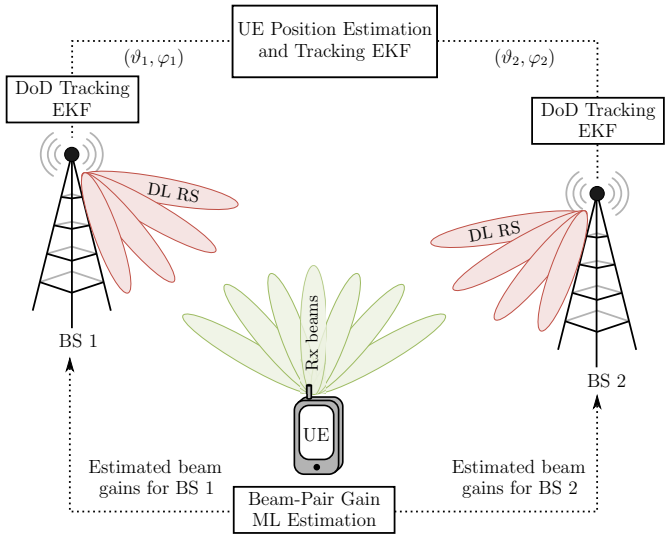

Fig. 1: Illustration of the UE positioning approach proposed in this paper. In particular, UEs estimate and feedback beams' gains of multiple BSs obtained from DL RSs by coherently combining the measured subcarriers. Only angles are used for positioning purposes. A single BS suffices in determining the 2D position of a UE given that its height is known. For 3D positioning at least two BSs are needed.

- BSs estimate and track the DoDs using reported gains from UEs. Optionally, UEs may also feedback the estimated variance of the reported gains.
- A central entity estimates and tracks the 3D positions of UEs.

III. Proposed Maximum Likelihood Estimation of Beam-Pair Gain

Let us first rewrite (1) in a more compact form:

$$\boldsymbol{y}_{i,j} = \tilde{\boldsymbol{b}}_f(\tau_{i,j})\beta_{i,j} + \boldsymbol{n}_{i,j}, \tag{3}$$

where $\tilde{\boldsymbol{b}}_f(\tau_{i,j}) \in \mathbb{C}^{\mathcal{M}_f}$ and $\beta_{i,j} \in \mathbb{C}$ are given by

$$\tilde{\boldsymbol{b}}_f(\tau_{i,j}) = \boldsymbol{S}\boldsymbol{b}_f(\tau_{i,j}), \tag{4}$$

$$\beta_{i,j} = b^i_{\text{UE}}(\vartheta_a, \varphi_a) b^j_{\text{BS}}(\vartheta_d, \varphi_d)\gamma_{i,j}. \tag{5}$$

Let also the unknown parameter vector be given by $\boldsymbol{\Theta}_{i,j} = [\tau_{i,j}, g_{i,j}, \phi_{i,j}, \sigma^2_{i,j}]^T$, where $g_{i,j} \in \mathbb{R}$ and $\phi_{i,j} \in [0, 2\pi)$ denote the magnitude (or gain) and phase of $\beta_{i,j}$, respectively. Note that $g_{i,j}$ and $\phi_{i,j}$ are related to the magnitudes and phases of $b^i_{\text{UE}}(\vartheta_a, \varphi_a)$, $b^j_{\text{BS}}(\vartheta_d, \varphi_d)$, and $\gamma_{i,j}$ by

$$g_{i,j} = g^i_{\text{UE}}(\vartheta_a, \varphi_a)\, g^j_{\text{BS}}(\vartheta_d, \varphi_d)\, g_{\gamma_{i,j}}, \tag{6}$$

$$\phi_{i,j} = \phi^i_{\text{UE}} + \phi^j_{\text{BS}} + \phi_{\gamma_{i,j}}. \tag{7}$$

To find the MLE of the beam-pair $g_{i,j}$, and more generally that of $\boldsymbol{\Theta}_{i,j}$, we start by writing the log-likelihood function of $\boldsymbol{\Theta}_{i,j}$ given $\boldsymbol{y}_{i,j}$, as

$$\ell(\boldsymbol{\Theta}_{i,j}|\boldsymbol{y}_{i,j}) = -\mathcal{M}_f \ln \pi - \mathcal{M}_f \ln \sigma^2_{i,j} - \frac{1}{\sigma^2_{i,j}} \|\boldsymbol{y}_{i,j} - \boldsymbol{\mu}(\boldsymbol{\Theta}_{i,j})\|^2, \tag{8}$$

where $\boldsymbol{\mu}(\boldsymbol{\Theta}_{i,j}) = \tilde{\boldsymbol{b}}_f(\tau_{i,j})\beta_{i,j}$. A general and convenient expression for the derivative of a complex-circular Gaussian probability density function (pdf) can be found in [12, Ch.15]. It follows that

$$\begin{aligned}\frac{\partial \ell(\boldsymbol{\Theta}_{i,j}|\boldsymbol{y}_{i,j})}{\partial [\boldsymbol{\Theta}_{i,j}]_n} &= -\text{tr}\left\{ \boldsymbol{C}_y^{-1}(\boldsymbol{\Theta}_{i,j}) \frac{\partial \boldsymbol{C}_y(\boldsymbol{\Theta}_{i,j})}{\partial [\boldsymbol{\Theta}_{i,j}]_n} \right\} \\ &+ (\boldsymbol{y}_{i,j} - \boldsymbol{\mu}(\boldsymbol{\Theta}_{i,j}))^H \boldsymbol{C}_y^{-1}(\boldsymbol{\Theta}_{i,j}) \frac{\partial \boldsymbol{C}_y(\boldsymbol{\Theta}_{i,j}}{\partial [\boldsymbol{\Theta}_{i,j}]_n} \\ &\quad \times \boldsymbol{C}_y^{-1}(\boldsymbol{\Theta}_{i,j}) (\boldsymbol{y}_{i,j} - \boldsymbol{\mu}(\boldsymbol{\Theta}_{i,j})) \\ &+ 2\Re\left\{ (\boldsymbol{y}_{i,j} - \boldsymbol{\mu}(\boldsymbol{\Theta}_{i,j}))^H \boldsymbol{C}_y^{-1}(\boldsymbol{\Theta}_{i,j}) \frac{\partial \boldsymbol{\mu}(\boldsymbol{\Theta}_{i,j})}{\partial [\boldsymbol{\Theta}_{i,j}]_n} \right\}, \end{aligned} \tag{9}$$

where $\boldsymbol{C}_y(\boldsymbol{\Theta}_{i,j}) = \sigma^2_{i,j}\boldsymbol{I}$ due to the independent and identically distributed (iid) assumption on the measurement noise $\boldsymbol{n}_{i,j}$. Equating the above derivative to zero yields the following expression for the MLE of the beam-pair gain:

$$\hat{g}_{i,j} = \frac{1}{\|\tilde{\boldsymbol{b}}_f(\hat{\tau}_{i,j})\|^2} \Re\left\{ \boldsymbol{y}^H_{i,j} \tilde{\boldsymbol{b}}_f(\hat{\tau}_{i,j}) \text{e}^{\text{j}\hat{\phi}_{i,j}} \right\}. \tag{10}$$

Here, $\hat{\tau}_{i,j}$ and $\hat{\phi}_{i,j}$ denote the MLEs of the delay and beam-pair phase. They are found by equating (9) to zero and solving for $\tau_{i,j}$ and $\phi_{i,j}$, yielding:

$$\hat{\tau}_{i,j} = \arg\max_{\tau_{i,j}} \frac{\tilde{\boldsymbol{b}}^H_f(\tau_{i,j}) \boldsymbol{R}_y \tilde{\boldsymbol{b}}_f(\tau_{i,j})}{\|\tilde{\boldsymbol{b}}_f(\tau_{i,j})\|^2}, \tag{11}$$

$$\hat{\phi}_{i,j} = \arctan\left\{ -\frac{\Im\left\{ \boldsymbol{y}^H_{i,j} \tilde{\boldsymbol{b}}_f(\hat{\tau}_{i,j}) \right\}}{\Re\left\{ \boldsymbol{y}^H_{i,j} \tilde{\boldsymbol{b}}_f(\hat{\tau}_{i,j}) \right\}} \right\}. \tag{12}$$

Here, $\boldsymbol{R}_y \in \mathbb{C}^{\mathcal{M}_f \times \mathcal{M}_f}$ denotes the sample correlation matrix of $\boldsymbol{y}_{i,j}$, i.e. $\boldsymbol{R}_y = \boldsymbol{y}_{i,j}\boldsymbol{y}^H_{i,j}$. Finally, the MLE of the measurement noise variance can be shown to be given by

$$\hat{\sigma}^2_{i,j} = \frac{1}{\mathcal{M}_f} \|\boldsymbol{y}_{i,j} - \boldsymbol{\mu}(\hat{\boldsymbol{\Theta}}_{i,j})\|^2. \tag{13}$$

The MLE of the beam-pair gain in (10) may be understood as a maximum ratio combining (MRC) since the phase introduced by the channel (and RF-chains) on each subcarrier is corrected, thus leading to a coherent combination of each subcarrier's gain.

It follows from (10)-(11) as well as (8) that $\hat{g}_{i,j}$ is Gaussian distributed, asymptotically unbiased and statistically efficient. The (asymptotic) mean and variance of $\hat{g}_{i,j}$ now follow from the Cramér-Rao bound (CRB) results in [11, Ch.4] expressed as

$$\mu(\hat{g}_{i,j}) = g_{i,j} \tag{14}$$

$$\text{var}(\hat{g}_{i,j}) = \frac{\sigma^2_{i,j}}{2\|\tilde{\boldsymbol{b}}_f(\tau_{i,j})\|^2}. \tag{15}$$

In the next section, the MLEs of a set of beam-pairs, and corresponding estimation variances, are employed for tracking the DoDs between a UE and multiple BSs, and for subsequent 3D UE position estimation.

IV. Proposed Extended Kalman Filter

A. EKF for DoD Estimation and Tracking

Let $\hat{g}_{i^*,j^*} \in \mathbb{R}$ denote the largest estimated beam-pair gain, i.e. $(i^*, j^*) = \arg\max_{i,j} \hat{g}_{i,j}$. Let also $\hat{\boldsymbol{g}} = [\hat{g}_{i^*,1}, \ldots, \hat{g}_{i^*,\mathcal{M}_{\rm BS}}]^T$ denote the estimated beam-pairs for a fixed UE beam and $\mathcal{M}_{\rm BS}$ BS beams. From the results in Section III it follows that vector $\hat{\boldsymbol{g}} \in \mathbb{R}^{\mathcal{M}_{\rm BS}}$ is Gaussian distributed with the following (asymptotic) mean and covariance matrix

$$\boldsymbol{\mu}_{\hat{g}} = \boldsymbol{g}_{\rm BS}(\vartheta_d, \varphi_d)\alpha, \tag{16}$$

$$\boldsymbol{C}_{\hat{g}} = \text{diag}\left\{ \frac{\sigma^2_{i^*,1}}{2\|\tilde{\boldsymbol{b}}_f(\tau_{i^*,1})\|^2}, \ldots, \frac{\sigma^2_{i^*,\mathcal{M}_{\rm BS}}}{2\|\tilde{\boldsymbol{b}}_f(\tau_{i^*,\mathcal{M}_{\rm BS}})\|^2} \right\}. \tag{17}$$

Here, $\alpha \in \mathbb{R}$ is an unknown scaling, and is given by $\alpha = g^{i^*}_{\rm UE}(\vartheta_a, \varphi_a)\, g_{\gamma_{i^*}}$ (see also (6)). In particular, the magnitude of the channels' path-weight corresponding to the beam-pair (i^*, j), and denoted by $g_{\gamma_{i^*,j}}$, is assumed to be independent of the BS' beams. More precisely, the proposed DoD-EKF assumes that $g_{\gamma_{i^*,1}} = g_{\gamma_{i^*,2}} = \ldots g_{\gamma_{i^*,\mathcal{M}_{\rm BS}}}$. In practice, such an assumption means that the radio channels between a *fixed* UE beam and all BS beams are identical. Typically, this holds true in practice.

Let us now consider the expressions for the DoD-EKF. We employ the so-called information-form EKF, which is known to be computationally more efficient than the corresponding Kalman-gain formulation when the dimension of the state-vector is larger than that of the measurement vector. This follows from the relationship between EKF and Gauss-Newton iteration of the maximum a posteriori (MAP) estimator [13, Ch.A3], [14]. In particular, let the state vector for the DoD-EKF be $\boldsymbol{s} = [\vartheta, \varphi, \Delta\vartheta, \Delta\varphi]^{\rm T}$, where $\Delta\vartheta$ and $\Delta\varphi$ denote the rate-of-change of ϑ and φ, respectively. The prediction step of the DoD-EKF is then

$$\boldsymbol{s}^-[n] = \boldsymbol{F}\boldsymbol{s}^+[n-1] \tag{18}$$

$$\boldsymbol{C}^-[n] = \boldsymbol{F}\boldsymbol{C}^+[n-1]\boldsymbol{F}^{\rm T} + \boldsymbol{Q}, \tag{19}$$

where $\boldsymbol{F} \in \mathbb{R}^{4\times4}$, $\boldsymbol{C} \in \mathbb{R}^{4\times4}$, and $\boldsymbol{Q} \in \mathbb{R}^{4\times4}$ denote the state-transition matrix, state covariance matrix, and state-noise covariance matrix, respectively. Matrices $\boldsymbol{F}$ and $\boldsymbol{Q}$ can be found from [15, Ch.2] by noting that we have employed a continuous white-noise acceleration model for the state-dynamics. The update step of the DoD-EKF is

$$\boldsymbol{C}^+[n] = \left(\boldsymbol{C}^-[n]^{-1} + \boldsymbol{\mathcal{I}}(\boldsymbol{s}^-[n])\right)^{-1} \tag{20}$$

$$\Delta\boldsymbol{s}[n] = \boldsymbol{C}^+[n]\, \boldsymbol{q}(\boldsymbol{s}^-[n]) \tag{21}$$

$$\boldsymbol{s}^+[n] = \boldsymbol{s}^-[n] + \Delta\boldsymbol{s}[n], \tag{22}$$

where $\boldsymbol{\mathcal{I}}(\boldsymbol{s}^-[n]) \in \mathbb{R}^{4\times4}$ and $\boldsymbol{q}(\boldsymbol{s}^-[n]) \in \mathbb{R}^4$ denote the observed Fisher information matrix (FIM) and score-function of the likelihood function of (ϑ_d, φ_d) given $\hat{\boldsymbol{g}}$ evaluated at $\boldsymbol{s}^-[n]$, respectively.

Under so-called regularity conditions of the likelihood function [16, Ch.6], the MLE is asymptotically unbiased and its (asymptotic) error covariance matrix equals the inverse of the FIM. Hence, one may employ the error covariance matrix, and gradient, of the MLE of (ϑ_d, φ_d) in place of $\boldsymbol{\mathcal{I}}(\boldsymbol{s}^-[n])$ and $\boldsymbol{q}(\boldsymbol{s}^-[n])$, respectively [13, Ch.A3], [14].

In particular, the log-likelihood function of $\boldsymbol{\Theta}$ given $\hat{\boldsymbol{g}}$ is given by

$$\ell(\boldsymbol{\Theta}|\hat{\boldsymbol{g}}) = -\frac{\mathcal{M}_{\rm BS}}{2}\ln 2\pi - \frac{\mathcal{M}_{\rm BS}}{2}\ln\tilde{\sigma}^2 - \ln\det\boldsymbol{C}_{\hat{g}} \tag{23}$$

$$- \frac{1}{2\tilde{\sigma}^2}(\hat{\boldsymbol{g}} - \boldsymbol{g}_{\rm BS}(\vartheta_d, \varphi_d))^T\boldsymbol{C}^{-1}_{\hat{g}}(\hat{\boldsymbol{g}} - \boldsymbol{g}_{\rm BS}(\vartheta_d, \varphi_d)). \tag{24}$$

Solving for $\tilde{\sigma}^2$ and replacing the resulting MLE in (23) yields:

$$\ell_c(\vartheta_d, \varphi_d|\hat{\boldsymbol{g}}) = -\frac{\mathcal{M}_{\rm BS}}{2}\ln 2\pi + \frac{\mathcal{M}_{\rm BS}}{2}\ln\mathcal{M}_{\rm BS} - \ln\det\boldsymbol{C}_{\hat{g}}$$
$$- \frac{\mathcal{M}_{\rm BS}}{2}\ln(\hat{\boldsymbol{g}} - \boldsymbol{g}_{\rm BS}(\vartheta_d, \varphi_d))^T\boldsymbol{C}^{-1}_{\hat{g}}(\hat{\boldsymbol{g}} - \boldsymbol{g}_{\rm BS}(\vartheta_d, \varphi_d)). \tag{25}$$

Taking $\exp\{\ell_c(\vartheta_d, \varphi_d|\hat{\boldsymbol{g}})\}$, since it does not change the maximum of (25), allows us to find the following expressions for the gradient and Hessian of the MLE of (ϑ_d, φ_d):

$$[\boldsymbol{q}(\vartheta_d, \varphi_d)]_1 = \left(\frac{\partial\boldsymbol{g}_{\rm BS}(\vartheta_d, \varphi_d)}{\partial\vartheta_d}\right)^T\boldsymbol{C}^{-1}_{\hat{g}}\,(\hat{\boldsymbol{g}} - \boldsymbol{g}_{\rm BS}(\vartheta_d, \varphi_d)) \tag{26}$$

$$[\boldsymbol{q}(\vartheta_d, \varphi_d)]_2 = \left(\frac{\partial\boldsymbol{g}_{\rm BS}(\vartheta_d, \varphi_d)}{\partial\varphi_d}\right)^T\boldsymbol{C}^{-1}_{\hat{g}}\,(\hat{\boldsymbol{g}} - \boldsymbol{g}_{\rm BS}(\vartheta_d, \varphi_d)) \tag{27}$$

$$[\boldsymbol{\mathcal{I}}(\vartheta_d, \varphi_d)]_{1,2} = \left(\frac{\partial\boldsymbol{g}_{\rm BS}(\vartheta_d, \varphi_d)}{\partial\vartheta_d}\right)^T\boldsymbol{C}^{-1}_{\hat{g}}\frac{\partial\boldsymbol{g}_{\rm BS}(\vartheta_d, \varphi_d)}{\partial\varphi_d}. \tag{28}$$

Note that we have used a first-order approximation of the Hessian since it equals, up to a scaling due to noise variance, the FIM for (ϑ_d, φ_d). It should also be noted that in practice an estimate of $\boldsymbol{C}_{\hat{g}}$ is used. Such an estimate is found by using (11) and (13) in (17), but requires reporting such estimates to the BSs, in addition to the beam-pair gains.

B. EKF for UE Positioning

The DoD estimates tracked by the DoD-EKF can be assumed to be given by

$$\begin{bmatrix}\hat{\vartheta}_k \\ \hat{\varphi}_k\end{bmatrix} \sim \mathcal{N}\left(\begin{bmatrix}\vartheta_k \\ \varphi_k\end{bmatrix}, \boldsymbol{C}_k\right), \tag{29}$$

where the subscript k denotes the BS index. We note that the covariance $\boldsymbol{C}_k \in \mathbb{R}^{2\times2}$ equals the upper-left (2×2) block of $\boldsymbol{C}^+[n]$ in the DoD-EKF, and it is assumed to be angle-independent. Such an assumption greatly simplifies the proposed Pos-EKF. In particular, let the state vector be given by $\boldsymbol{s}_{\rm UE} = [x_{\rm UE}, y_{\rm UE}, z_{\rm UE}, v_x, v_y, v_z]^{\rm T}$, where (v_x, v_y, v_z) denote the components of the velocity vector along the Cartesian unit vectors. The prediction step of the Pos-EKF is then

$$\boldsymbol{s}^-_{\rm UE}[n] = \boldsymbol{F}_{\rm UE}\boldsymbol{s}^+_{\rm UE}[n-1] \tag{30}$$

$$\boldsymbol{C}^-_{\rm UE}[n] = \boldsymbol{F}_{\rm UE}\boldsymbol{C}^+_{\rm UE}[n-1]\boldsymbol{F}^{\rm T}_{\rm UE} + \boldsymbol{Q}_{\rm UE}, \tag{31}$$

where $\boldsymbol{F}_{\mathrm{UE}} \in \mathbb{R}^{6\times 6}$, $\boldsymbol{C}_{\mathrm{UE}} \in \mathbb{R}^{6\times 6}$, and $\boldsymbol{Q}_{\mathrm{UE}} \in \mathbb{R}^{6\times 6}$ denote the state-transition matrix, state covariance matrix, and state-noise covariance matrix, respectively; see [15, Ch.2] for details. The update step of the Pos-EKF is now

$$\boldsymbol{C}^{+}_{\mathrm{UE}}[n] = \left(\boldsymbol{C}^{-}_{\mathrm{UE}}[n]^{-1} + \boldsymbol{\mathcal{I}}_{\mathrm{UE}}(\boldsymbol{s}^{-}_{\mathrm{UE}}[n])\right)^{-1} \tag{32}$$

$$\Delta\boldsymbol{s}_{\mathrm{UE}}[n] = \boldsymbol{C}^{+}_{\mathrm{UE}}[n]\, \boldsymbol{q}_{\mathrm{UE}}(\boldsymbol{s}^{-}_{\mathrm{UE}}[n]) \tag{33}$$

$$\boldsymbol{s}^{+}_{\mathrm{UE}}[n] = \boldsymbol{s}^{-}_{\mathrm{UE}}[n] + \Delta\boldsymbol{s}_{\mathrm{UE}}[n], \tag{34}$$

where $\boldsymbol{\mathcal{I}}_{\mathrm{UE}}(\boldsymbol{s}^{-}_{\mathrm{UE}}[n]) \in \mathbb{R}^{6\times 6}$ and $\boldsymbol{q}_{\mathrm{UE}}(\boldsymbol{s}^{-}_{\mathrm{UE}}[n]) \in \mathbb{R}^{6}$ denote the observed FIM and gradient of the log-likelihood function of UE position given DoD estimates from multiple BSs.

Let $\boldsymbol{m} \in \mathbb{R}^{2K}$ denote the estimated DoDs of K BSs for a given UE. It follows from (29) that $\boldsymbol{m} \sim \mathcal{N}\left(\boldsymbol{\mu}(\boldsymbol{p}), \boldsymbol{C}\right)$, where

$$\boldsymbol{\mu}(\boldsymbol{p}) = \left[\vartheta_1(\boldsymbol{p}), \varphi_1(\boldsymbol{p}), \ldots, \vartheta_K(\boldsymbol{p}), \varphi_K(\boldsymbol{p})\right]^{\mathrm{T}} \tag{35}$$

$$\boldsymbol{C} = \mathrm{blkdiag}\left\{\boldsymbol{C}_1, \ldots, \boldsymbol{C}_K\right\}. \tag{36}$$

Here, $\boldsymbol{p} \in \mathbb{R}^3$ denotes the 3D Cartesian coordinate of a UE's position and $\mathrm{blkdiag}\{\cdot\}$ denotes a block-diagonal matrix. The DoDs are related to the UE's position through:

$$\vartheta_k(\boldsymbol{p}) = \arctan\left(\frac{-\Delta z_k}{d_{2D_k}}\right) + \pi/2 \tag{37}$$

$$\varphi_k(\boldsymbol{p}) = \arctan 2\left(\Delta y_k, \Delta x_k\right), \tag{38}$$

where $d_{2D_k} = \sqrt{\Delta x_k^2 + \Delta y_k^2}$, $\Delta x_k = x_{\mathrm{UE}} - x_{\mathrm{BS}_k}$, $\Delta y_k = y_{\mathrm{UE}} - y_{\mathrm{BS}_k}$, and $\Delta z_k = z_{\mathrm{UE}} - z_{\mathrm{BS}_k}$. The gradient of the log-likelihood function of $\boldsymbol{p}$ given $\boldsymbol{m}$, and respective observed FIM, now follow from [12, Ch.3]

$$[\boldsymbol{q}_{\mathrm{UE}}(\boldsymbol{p})]_m = \left(\frac{\partial\boldsymbol{\mu}(\boldsymbol{p})}{\partial[\boldsymbol{p}]_m}\right)^{\mathrm{T}} \boldsymbol{C}^{-1}\left(\boldsymbol{m} - \boldsymbol{\mu}(\boldsymbol{p})\right) \tag{39}$$

$$[\boldsymbol{\mathcal{I}}_{\mathrm{UE}}(\boldsymbol{p})]_{m,n} \approx \left(\frac{\partial\boldsymbol{\mu}(\boldsymbol{p})}{\partial[\boldsymbol{p}]_m}\right)^{\mathrm{T}} \boldsymbol{C}^{-1}\frac{\partial\boldsymbol{\mu}(\boldsymbol{p})}{\partial[\boldsymbol{p}]_n}. \tag{40}$$

V. Numerical Results

A. Deployment Scenario

We consider a scenario where two BSs and a UE are deployed in an environment resembling a maritime port. This is a common envisioned deployment for industrial IoT applications based on mmW cellular networks. The UE represents a container-hauling truck. Fig. 2 illustrates the considered environment as well as the locations of BSs and UE. In particular, BSs are deployed at a height of $50\,\mathrm{m}$ while that of the UE is $1.5\,\mathrm{m}$.

In this numerical study a mmW system operating at $39\,\mathrm{GHz}$ and with a reference signal bandwidth of $10\,\mathrm{MHz}$ is considered. The subcarrier spacing is $120\,\mathrm{kHz}$ and the resulting number of subcarriers available for transmitting DL-RSs is 80. The power budget at each BS is $21\,\mathrm{dBm}$. Each BS transmits DL-RSs through 64 beams towards different directions. In particular, such BS beams span 40° both in elevation and azimuth, and the $3\,\mathrm{dB}$ beamwidth is $\approx 3^\circ$. DL-RSs for different beams and BSs are assumed to be scheduled in orthogonal radio resources (TDM or CDM). The UE receives DL-RSs from 52 beams spanning 360° in azimuth and a fixed direction ($\approx 75^\circ$) in co-elevation. The $3\,\mathrm{dB}$ beamwidth is $\approx 6^\circ$ in azimuth and $\approx 40^\circ$ in elevation. The maximum gains of the BS and UE beams are $\approx$30 dBi and $\approx$17 dBi, respectively. It is assumed that the UE estimates the gains for all 64×52 beam-pairs, for both BSs, in $160\,\mathrm{ms}$, after which it feedbacks the highest beam-pair gains.

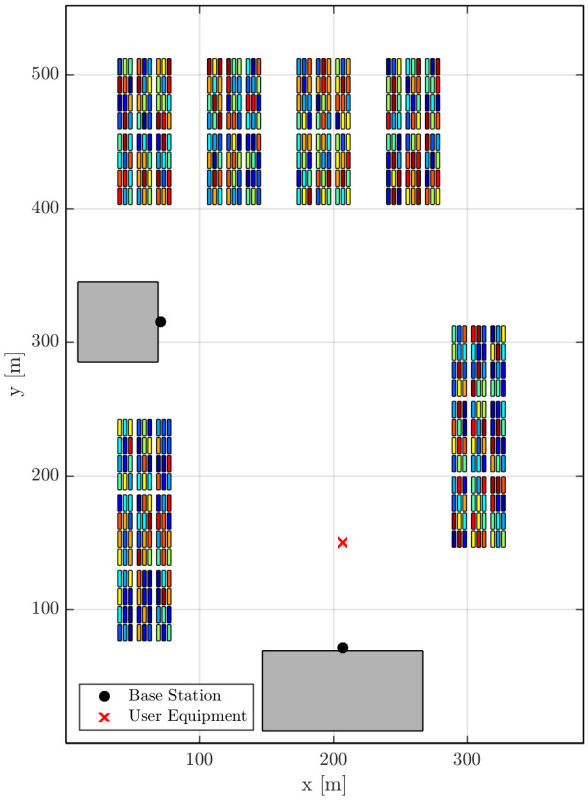

Fig. 2: Illustration of the simulation environment for assessing the performance of the proposed two-stage EKF in a maritime port area. The considered port area consists of two buildings (gray rectangles) and blocks of piled metallic containers (coloured rectangles). The radio channels between a UE (red cross) and BSs (black dots) are modeled according to the METIS ray-tracing channel model [17].

The radio channel between UE and BSs follows that of METIS ray-tracing channel model [17]. Hence, all multipath components between UE and BSs are taken into account in the DL-RS measurements, and re-calculated for every UE position. In particular, buildings and containers are modeled as metal structures. Their heights are $52\,\mathrm{m}$ and $10\,\mathrm{m}$, respectively. For ground reflections, a medium-dry model is used; see [17] for details.

B. Performance of the Proposed Positioning Scheme

The performance of the proposed two-stage EKF is assessed by considering a UE moving with a velocity of $2\,\mathrm{m\,s^{-1}}$. The UE moves along a $100\,\mathrm{m}$-long straight trajectory from south to north. The starting position of the UE is illustrated in Fig. 2. The southernmost BS is north-facing while the northernmost BS has a 50° orientation clockwise from East-side. The UE feedbacks estimates for the beam-pair gains every $160\,\mathrm{ms}$.

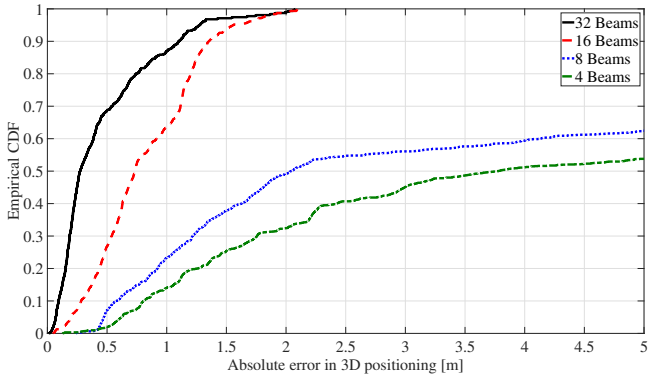

Fig. 3: Empirical CDF of 3D positioning error obtained using the proposed method for a varying number of feedback beam-pair gain estimates. Sub-meter accuracy is achieved in 90% of the user's trajectory given that 32 beam-pair gain estimates are feedback. Attaining an identical accuracy and reducing the amount of feedback beam-pair gain estimates requires increasing the bandwidth of DL RS from the current 10 MHz.

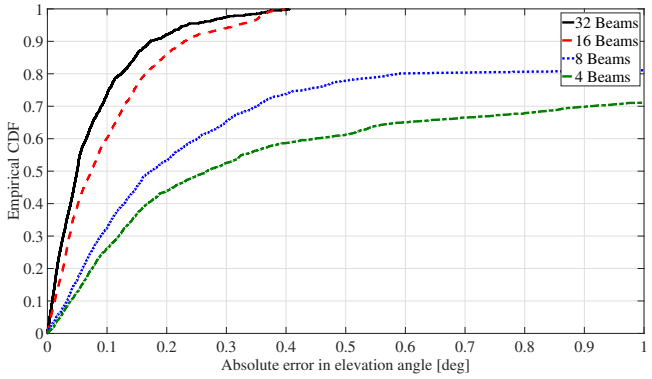

Fig. 4: Empirical CDF of elevation-angle error obtained using the proposed method for a varying number of feedback beam-pair gain estimates.

Initialization of the DoD-EKF and Pos-EKF follows that in [18].

In particular, we consider the case when the number of feedback beam-pairs is 32, 16, 8, and 4. Note that the performance of the proposed positioning scheme with respect to (wrt) the number of feedback beam-pairs is heavily dependent on the shape of the BSs' transmit beams as well as relative BSs-UE location. Fig. 3 illustrates the cumulative distribution function (CDF) of the 3D positioning error while that of elevation-angle and azimuth-angle are given in Fig. 4 and Fig. 5, respectively. Results show that sub-meter positioning accuracy is achieved in 90% of user's trajectory given that 32 beam-pair gain estimates are reported. For 16 beam-pair gain estimates sub-meter accuracy is attained in 60% of the route. Reporting 8 or 4 beams-pair gains does not suffice in reaching sub-meter 3D positioning accuracy with the proposed scheme.

VI. Conclusion

We have proposed a 5G mmW user positioning method that consists in reporting maximum likelihood estimates of beam-pair gains acquired by means of beamformed DL RSs. Such

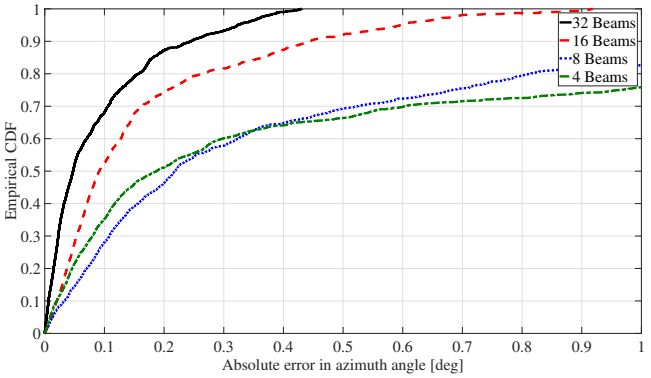

Fig. 5: Empirical CDF of azimuth-angle error obtained using the proposed method for a varying number of feedback beam-pair gain estimates.

estimates may be understood as a maximum ratio combining of the subcarriers modulated by the RSs. A parametric model for the radio channel was employed, and the combined frequency response of Tx-Rx RF-chains was assumed calibrated, or frequency-flat. A two-stage EKF was also proposed for estimating and tracking the 3D position of users based on feedback beam-pair gain estimates. In particular, each BS tracks the DoD of the LoS path to a given user by means of a first-stage EKF. Subsequently, DoD estimates from multiple BSs are fused into 3D position estimates of the users' locations. We have assessed the performance of the proposed positioning scheme on a realistic ray-tracing based environment resembling a maritime port with metal containers. The focus was in industrial IoT applications operating at 39 GHz and with a 10 MHz RS bandwidth. Results show that sub-meter positioning accuracy is achieved in 60% of the user's trajectory given that 16 beam-pair gain estimates are reported. Increasing the number of reported gain estimates to 32 leads to sub-meter accuracy for 90% of the route. Our results allow one to design the capacity of the feedback channel for a given positioning accuracy.

References

[1] 3GPP, TR22.872, "Study on positioning use cases, stage 1," 2016. [Online]. Available: https://portal.3gpp.org/desktopmodules/Specifications/SpecificationDetails.aspx?specificationId=3280

[2] 3GPP, RP-172746, "New SID: study on NR positioning support," 2017. [Online]. Available: https://portal.3gpp.org/ngppapp/CreateTdoc.aspx?mode=view&contributionId=853821

[3] S. Sun, T. S. Rappaport, R. W. Heath, A. Nix, and S. Rangan, "MIMO for millimeter-wave wireless communications: beamforming, spatial multiplexing, or both?" *IEEE Communications Magazine*, vol. 52, no. 12, pp. 110–121, December 2014.

[4] 3GPP, TS38.214, "Physical layer procedures for data," 2018. [Online]. Available: https://portal.3gpp.org/desktopmodules/Specifications/SpecificationDetails.aspx?specificationId=3216

[5] E. Rastorgueva-Foi, M. Costa, M. Koivisto, K. Leppänen, and M. Valkama, "User positioning in mmW 5G networks using beam-RSRP measurements and Kalman filtering," 2018. [Online]. Available: https://arxiv.org/pdf/1803.09478.pdf

[6] S. Tsugawa, S. Jeschke, and S. E. Shladover, "A review of truck platooning projects for energy savings," *IEEE Transactions on Intelligent Vehicles*, vol. 1, no. 1, pp. 68–77, March 2016.

[7] S. Ellwanger and E. Wohlfarth, "Truck platooning application," in *2017 IEEE Intelligent Vehicles Symposium (IV)*, June 2017, pp. 966–971.

[8] C. Bergenheim, S. Shladover, and E. Coelingh, "Overview of platooning systems," in *Proceedings of the 19th ITS World Congress, Oct 22-26, Vienna, Austria*, 2012.

[9] Ministry of Transport (MOT) and Port of Singapore (PSA) Corporation, "Singapore to start truck platooning trials," Jan. 2017. [Online]. Available: https://www.globalpsa.com/assets/uploads/nr170109.pdf

[10] A. Molisch, "A generic model for MIMO wireless propagation channels in macro- and microcells," *IEEE Trans. Signal Proc.*, vol. 52, no. 1, pp. 61–71, Jan 2004.

[11] A. Richter, "Estimation of radio channel parameters: Models and algorithms," Ph.D. dissertation, Technische Universität Ilmenau, 2005, http://www.db-thueringen.de/servlets/DerivateServlet/Derivate-7407/ilm1-2005000111.pdf.

[12] S. Kay, *Fundamentals of Statistical Signal Processing: Estimation Theory*. Prentice-Hall Signal Processing Series, 1993.

[13] R. Merwe, "Sigma-Point Kalman Filters for Probabilistic Inference in Dynamic State-Space Models," Ph.D. dissertation, Electrical and Computer Engineering, Oregon Health & Science University, 2004. [Online]. Available: https://digitalcommons.ohsu.edu/cgi/viewcontent.cgi?article=1007&context=etd

[14] B. Bell and F. Cathey, "The iterated Kalman filter update as a Gauss-Newton method," *IEEE Trans. Automatic Control*, vol. 38, no. 2, pp. 294–297, Feb 1993.

[15] J. Hartikainen, A. Solin, and S. Särkkä, "Optimal filtering with Kalman filters and smoothers," 2011. [Online]. Available: http://becs.aalto.fi/en/research/bayes/ekfukf/documentation.pdf

[16] G. Casella and R. Berger, *Statistical Inference*, 2nd ed. Duxbury, 2002.

[17] METIS, "D1.4 Channel models," Feb. 2015. [Online]. Available: https://www.metis2020.com/wp-content/uploads/METIS_D1.4_v3.pdf

[18] M. Koivisto, M. Costa, J. Werner, K. Heiska, J. Talvitie, K. Leppänen, V. Koivunen, and M. Valkama, "Joint Device Positioning and Clock Synchronization in 5G Ultra-Dense Networks," *IEEE Trans. Wireless Comm.*, vol. 16, no. 5, pp. 2866–2881, May 2017.